Evaluation of relative efficiency of PDT photosensitizers in producing hydroxyl radicals and singlet oxygen in aqueous media using a UV–visible spectroscopy pNDA dosage

Clément Linger, Maxime Lancel, Marc Port

Evaluation of relative efficiency of PDT photosensitizers in producing hydroxyl radicals and singlet oxygen in aqueous media using a UV-visible spectroscopy pNDA dosage

Clément Linger[a,*], Maxime Lancel[a], Marc Port[a,*]

[a] *Équipe de Chimie Moléculaire du Laboratoire Génomique, Bioinformatique et Chimie Moléculaire (EA 7528), Conservatoire National des Arts et Métiers (CNAM), 2 rue Conté, 75003, HESAM Université , Paris, France*

Abstract

In order to improve the performance of PDT, it is important to develop new photosensitizers that induce the formation of both hydroxyl radicals and singlet oxygen. In this work, we developed and validated the experimental conditions and reproducibility for the evaluation of relative efficiency of hydroxyl radicals and singlet oxygen production by studying the bleaching of p−nitrosoaniline (pNDA) using a continuous flow UV-visible spectroscopy method in presence of photosensitizers in PBS media. Rapid data sampling made possible to analyze the kinetics of the bleaching and using a mathematical modeling. The pNDA dosage is specific of hydroxyl radicals' production without L-histidine and of singlet oxygen production in presence of L-histidine. A statistical approach is used to precisely evaluate the reliability of the results and to be able to compare different photosensitizers between them such as Methylene Blue and Brillant Blue G.

Keywords: PDT, pNDA, Methylene Blue, Brilliant Blue G, Singlet Oxygen, Hydroxyl Radicals, UV-Visible Dosage

1. Introduction

Photodynamic therapy (PDT) is a medical procedure mainly used in the treatment of cancers and complementary to existing treatments i.e. surgery, immunotherapy, radiotherapy or chemotherapy.

This medical procedure combines the use of a photosensitizers (PS) injected with a non-toxic dose either locally or systemically and light irradiation to

*Corresponding author

Email addresses: clement.linger@sorbonne-universite.fr (Clément Linger), marc.port@lecnam.net (Marc Port)

produce cytotoxic Reactive Oxygen Species (ROS) such as peroxides, superoxide, hydroxyl radical and singlet oxygen, which eradicate cancer cells [1]. The photophysical mechanism of PDT is inherently complex and is described by the production of the singlet state of the photosensitizers upon light irradiation of the ground state which is deexcited by fluorescence and interconversion of the system into a triplet state. One of the most commonly admitted pathways is illustrated by Figure 1. Because of their long lifetimes, triplet excited states can efficiently transfer energy to other molecules, which promotes the formation of ROS causing cytotoxicity. From there, two routes are possible [2]:

- the so-called type I reaction which generates radicals which induce the production of ROS such as superoxide anion ($O_2^{\bullet -}$), hydroxyl radical ($HO^{\bullet}$) via reaction with O_2 or FENTON reaction for example
- the so-called type II reaction which makes the oxygen, originally in a triplet state ($^3O_2$ or $^3\Sigma_g^-$), pass to a highly reactive singlet state ($^1O_2$ or $^1\Delta_g$).

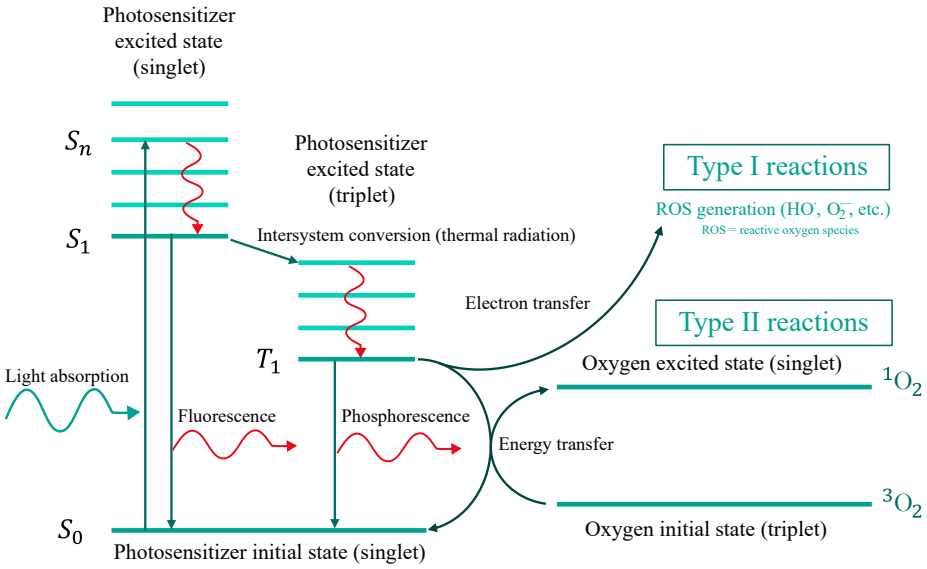

Figure 1: Supposed photosensitizer mechanims, adapted from [3].

The vast majority of photosensitizers interact with their biological surroundings by a type II mechanism. However, aggressive or drug resistant tumors are often characterized by having large regions with low partial oxygen pressure and therefore cells in hypoxic condition. Therefore, in order to improve the performance of PDT, it is important to develop PSs which may induce the formation of radical through type I reaction or through a mixed type I and type II mechanism [4].

Faced with this challenge, it is important to be able to quantify in a robust and simple way both the hydroxyl radicals and the singlet oxygen produced during a PDT procedure to characterize the properties and performance of a PS.

Different methods are described in the literature to quantify the production of singlet oxygen using fluorescent probes, for instance Singlet Oxygen Sensor Green (SOSG) [5], Aarhus sensor green (ASG) [6], dipropionic acid anthracene (DPAA) [7]) and dihydroethidium (DHE) or its mitochondria-targeted form Mito-SOX (Mito-DHE) [8] (cellular or mitochondrial $^1O_2$ quantification), UV probes such as 1,3-diphenylisobenzofuran (non-soluble in neat water [9]) and furfuryl alcohol [10], or singlet oxygen luminescence determination [11].

Few methods are applied to radicals' detection and most of them are described as non-specific regarding $^1O_2$. Among those techniques one could mention fluorescent probes such as dihydrorhodamine (DHR) devoted to $ONOO^-$ detection [8] and dichlorodihydrofluorescein diacetate (DCFH-DA) commonly used for intracellular H_2O_2 detection [8]. Other few components can be used with less convenient detection modalities (mass spectroscopy, HPLC, etc) such as Coumarin boronic acid (CBA) for $ONOO^-$ radicals [8].

The lack of specificity toward $^1O_2$ or radicals' detection often imply the use of scavengers for $^1O_2$, such as L-histidine [12], or for radicals especially $HO^\bullet$ with D-mannitol [13] for instance and $O_2^{\bullet -}$ with Superoxide Dismutases (SOD) [14]. Combination of different methods are also necessary to get all the description of the oxidation routes for a particular compound, with all the difficulties of quantification of ROS production according to different analytical methods used.

A method of determination was however used in photochemistry [15, 16] (and at list by one team in sonochemistry [17]) to quantify the production of singlet oxygen and hydroxyl radicals with the same UV spectrometric dosage in an aqueous media. It uses a reagent, p−nitrosoaniline (pNDA), which shows a large absorption at 440 nm, forming a yellow solution especially in water. In the presence of hydroxyl radicals, pNDA loses its absorbance ability, which allows to follow the radical production by spectrophotometry [18], following the mecanism already described by [19, 20] and presented in Figure 2a. On the other hand, pNDA reacts with L-histidine and still loses its absorbance ability, but only when L-histidine has been endoperoxidized by a singlet oxygen molecule. Thus, the production of singlet oxygen is also monitored in UV-visible [21]. The question of the mechanism of pNDA bleaching in presence of L-histidine is complex and is unresolved in the literature. In his original publication, Kraljić [21] proposes that the pNDA bleaching is a consequence of $^1O_2$ capture by the imidazole ring which results in the formation of a trans-annular peroxide intermediate $HistO_2$ capable of inducing the bleaching of pNDA. This endoperoxide is also described by [22]. To our knowledge, all publications using this assay method rely on the formation of this trans-annular peroxide. However, the exact reaction mechanism is still unclear, particularly concerning the chemical reactivity of this trans-annular peroxide intermediate. This reactivity and this mechanism have never been investigated to our knowledge. As the homolytic cleavage of endoperoxide bond by photolysis in known ([23] and [24]), a speculative mechanism can be proposed based on an attack of this biradical on the pNDA skeleton which explains its

loss of absorbance at 440 nm by loss of aromatic character (Figure 2b).

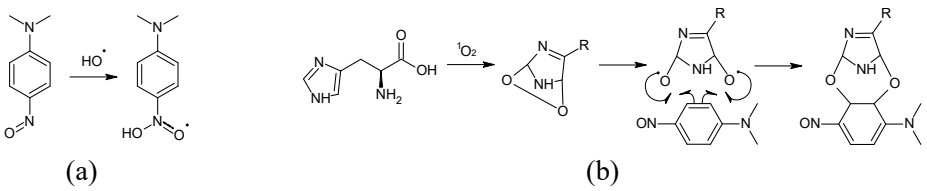

Figure 2: Supposed dosage mechanisms. (a) pNDA oxidation by hydroxyl radicals, adapted from [19, 20]. (b) L-histidine endoperoxidation adapted from [22] followed by a speculative mechanism

.

This pNDA method was notably investigated by Kraljić *et al.* in [21] to quantify singlet oxygen production. However, a few information is missing in this paper to reproduce perfectly the set up. Indeed, the photosensors concentrations and the precise excitation wavelength are not mentioned. Moreover, the potential of pNDA for radicals' detection is not developed in this original study. Some following papers use this method in their photosensors characterization such as [15] for vitamin K or [18] for 2-Anthraquinone sulfonate (AQS) and others propose to use pNDA for biochemically generated hydroxyl radicals [16]. However, the experimental conditions and set-up regarding pNDA use are incompletely described (pH control, acquisition mode or wavelength of study and rate of acquisition not mentioned).

Thus, we have here investigated the potential of this method to make the set up more reliable and reproducible . Preliminary data showed that manual sampling introduced too much disparity in the sampling times and too little sampling to obtain reproducible results. Consequently, we developed a continuous flow UV-visible determination device for both hydroxyl radicals and singlet oxygen detection. Rapid data sampling made possible by the continuous system allowed us to propose a mathematical modeling of the kinetics involved. Finally, we also propose a statistical approach to evaluate precisely the reliability of the results and to be able to compare different photosensitizers between them such as Methylene Blue (MB) and Brilliant Blue G (BBG).

To establish the proof of concept, we have chosen to study the excitement in red light of MB photosensitizer which is seems to have a great potential for application in PDT [25, 26, 27, 28]. Wavelength in the red or near-infrared spectrum (typically 600–900 nm) are especially adapted to clinical problems in oncology as these wavelengths penetrate much deeper and are therefore favored for deep-seated or large tumors. Moreover, MB is already referenced in the drug bank (DB09241) for the treatment of pediatric and adult patients with acquired methemoglobinemia.

Moreover, the photophysical properties of MB have been studied in detail showing that this photosensitizer can simultaneously induce type I and type II

reactions [29] (cf. Figure 3) and is therefore a PS of choice for our study.

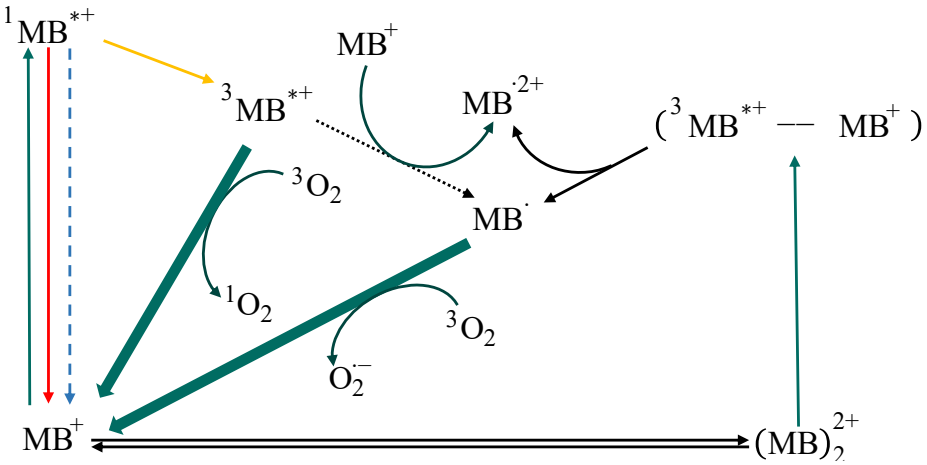

Figure 3: Partial photochemical reaction routes of MB, adapted from [29]. In green dotted line, light absorption; in blue short dashed lines, fluorescent deexcitation; in red mixed line, non-radiative deexcitation, in yellow long dashed line, triplet to singlet or singlet to triplet state transfer; in black large line, transition of interest in ROS production.

2. Materials and methods

2.1. Chemicals

N,*N*-dimethyl-4-nitrosoaniline (pNDA) and Methylene Blue were purchased from Sigma Aldrich (St. Louis, MO). Brilliant Blue G and L-histidine were purchased from Tokyo Chemical Industry (Europe). Sodium Azide was purchased from Acros Organics. The chemical structures of these reagents are given in Figure 10. All the other reagents were commercial product of analytical grade. All reagents were dissolved in PBS and conserved protected from light.

Phosphate Buffer Saline (PBS) was prepared in large volumes with potassium dihydrogenphosphate (KH_2PO_4) – 1.80 mM – disodium hydrogenphosphate (Na_2HPO_4) – 10.0 mM – sodium chloride (NaCl) – 137 mM – potassium chloride (KCl) – 2.70 mM. The pH was controlled at 7.4 ± 0.2.

2.2. Irradiation apparatuses

All light exposure experiments were done using a red LEDs crown containing 294 LEDs. The LEDs are furnished by Inspire (DichrOLED, France) and have a power of 0.1 W for an emission wavelength of 630 nm. The crown has then a power of 29.4 W. The wavelength emission was chosen to fit with Methylene Blue and Brilliant Blue G (the photosensors used) maximum absorption characteristics.

2.3. Kinetics UV-vis monitoring

The progress of each experiment is monitored by UV-vis at 440 nm. This one is either in *kinetics* mode for the flow monitoring (one point every 20 s) or in *photometric* mode for the point by point monitoring. If this is not specified, the analysis was performed in flow. The UV equipment is a UV-2600i spectrophotometer (Shimadzu). The quartz spectroscopic cells are supplied by Hellma (flow-through and static cuvettes), the pump is a peristaltic model (Heidolph Pumdrive 5001) and the tubing is made of perfluoroalkoxy alkane (PFA) or platinum cured silicon (Watson & Marlow tubing). A schematic representation of the set-up is given in Figure 4.

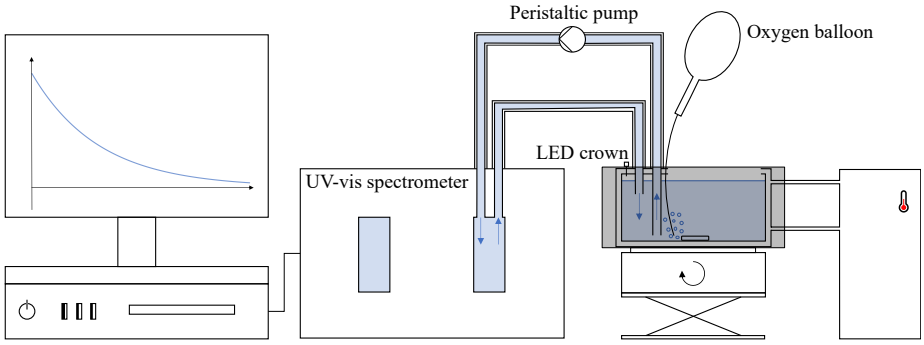

Figure 4: Set-up schematic representation.

2.4. Dosage Protocol

A fresh solution of pNDA (90 µM) and photo sensitizers (20 µM for MB and 17.5 µM for BBG) in PBS pH = 7.4 is mixed using a magnetic stirring (1,220 rpm) at 20 °C (regulated by a cryostat and the double envelope) under oxygen (balloon bubbling). L-histidine (5 mM) is optionally added depending on the required result. At the beginning of the experiment, the solution is equilibrated with the lab atmosphere and the balloon bubbling for 5 minutes under stirring. Later, the renewal is permitted by the balloon bubbling and the stirring. Therefore, the oxygen concentration can be considered as constant. Red LEDs irradiates the solution for 15 minutes. Each experiment is performed 6 times to obtain statistically relevant data.

2.5. Statistics

The statistical results are given in the form of p-value. These are the result of a Student's test evaluating the significance of the difference between the means of a series, done with R. Typically, the significance of the differences between the bleaching caused by two sensitizers is evaluated in this way. The laterality as well as the difference between the variances is also taken into account. The

results are considered significant if $p < 0.01$ (null hypothesis probability under 1%). The p-value is given between the different boxplot when relevant with the following code: *** if $p \leq 0.001$, ** if $p \leq 0.01$, * if $p \leq 0.05$, • if $p \leq 0.1$ and × if $p > 0.1$ (non-significant at all). p-values are also given in the case of linear regressions for fitting the experimental data with the models.

2.6. Dosage Modeling

The pNDA dosage has the asset to be usable for radicals' dosage and singlet oxygen dosage, in presence of L-histidine. We are presenting here a hypothetical modeling of the reaction mechanisms leading to the bleaching of the medium. The followed reaction is the disappearance of pNDA (and thus indirectly the formation of the oxidized species –pNDA). This part is thus divided between detection of singlet oxygen and hydroxyl radicals.

2.6.1. $^1O_2$ mechanism

We model the reaction mechanism (with $^1O_2$) like followed:

$$\mathrm{PS} + \mathrm{h}\nu \xrightarrow{k_1} \mathrm{PS}^* \quad \{1\}$$

$$\mathrm{PS}^* \xrightarrow{k_2} \mathrm{PS} + \mathrm{h}\nu_{F_1} \quad \{2\}$$

$$\mathrm{PS}^* \xrightarrow{k_3} \mathrm{PS} \quad \{3\}$$

$$\mathrm{PS}^* + {}^3\mathrm{O}_2 \xrightarrow{k_4} \mathrm{PS} + {}^1\mathrm{O}_2 \quad \{4\}$$

$${}^1\mathrm{O}_2 \xrightarrow{k_5} {}^3\mathrm{O}_2 \quad \{5\}$$

$${}^1\mathrm{O}_2 \xrightarrow{k_6} {}^3\mathrm{O}_2 + \mathrm{h}\nu_{F_2} \quad \{6\}$$

$${}^1\mathrm{O}_2 + \mathrm{Hist} \xrightarrow{k_7} \mathrm{HistO}_2 \quad \{7\}$$

$$\mathrm{HistO}_2 + \mathrm{pNDA} \xrightarrow{k_8} -\mathrm{pNDA} \quad \{8\}$$

$$\mathrm{pNDA} \xrightarrow{k_9} -\mathrm{pNDA} \quad \{9\}$$

We then assume than $^1O_2$ is not stable in the medium (steady state hypothesis) and we are considering it as a reactive intermediate. $\frac{\mathrm{d}[^1\mathrm{O}_2]}{\mathrm{d}t} = 0$ and $v_5 + v_6 + v_7 = v_4$. For v_7, we are considering L-histidine in wide excess, i.e. $[\mathrm{Hist}] = [\mathrm{Hist}]_0$ and then $v_7 = k_7^{'}[^1\mathrm{O}_2]$

Finally,

$$[^1\mathrm{O}_2] = \frac{k_4[^3\mathrm{O}_2][\mathrm{PS}^*]}{k_5 + k_6 + k_7^{'}} \quad (1)$$

The interesting speed here is the rate of disappearance of pNDA, neglecting its auto-oxidation [9]. Therefore:

$$v = v_8 = k_8[\mathrm{HistO_2}][\mathrm{pNDA}] \tag{2}$$

In the reaction 7, $^1O_2$ is very reactive and does not exist in the medium, and L-histidine is in wide excess. Therefore, we are considering $[\mathrm{HistO_2}] = [^1O_2]$, as proposed by Kraljić *et al.* [21].

Finally:

$$v = -\frac{\mathrm{d[pNDA]}}{\mathrm{d}t} = k_8[^1O_2][\mathrm{pNDA}] = \frac{k_8 k_4}{k_5 + k_6 + k_7^{'}}[^3O_2][\mathrm{PS^*}][\mathrm{pNDA}] = K[\mathrm{pNDA}] \tag{3}$$

with $\boxed{K = k_8[^1O_2] = \frac{k_8 k_4}{k_5 + k_6 + k_7^{'}}[^3O_2][\mathrm{PS^*}]}$.

The kinetic law is then linearizable via $\boxed{\ln \frac{[\mathrm{pNDA}]_0}{[\mathrm{pNDA}]_t} = Kt}$.

2.6.2. $HO^\bullet$ mechanism

It is demonstrated in the literature that the bleaching of pNDA in the medium is due to $HO^\bullet$, as pNDA do not react with singlet oxygen, superoxide anions or others peroxy compounds [20]. Two superoxide radicals can combine together to form H_2O_2 and oxygen (equation 13). Under light exposure, H_2O_2 produce hydroxyl radicals by photolysis [30] (equation 14). This kind of mechanism has been already described in [18]. Moreover, the experimental curves seem to confirm the first order hypothesis.

The modeling is in fact very close to the previous one (with a step involving the photolysis of hydrogen peroxide produced by combination of two superoxide ions [30]) and each remark can be adapted to this model.

$$\mathrm{PS} + \mathrm{h\nu} \xrightarrow{\mathrm{k_1}} \mathrm{PS^*} \quad \{1\}$$

$$\mathrm{PS^*} \xrightarrow{\mathrm{k_2}} \mathrm{PS} + \mathrm{h\nu_{F_1}} \quad \{2\}$$

$$\mathrm{PS^*} \xrightarrow{\mathrm{k_3}} \mathrm{PS} \quad \{3\}$$

$$\mathrm{PS^* + PS} \xrightarrow{\mathrm{k_{10}}} \mathrm{PS^\bullet + PS^{\bullet +}} \quad \{10\}$$

$$\mathrm{PS^\bullet + {}^3O_2} \xrightarrow{\mathrm{k_{11}}} \mathrm{PS + {O_2}^{\bullet -}} \quad \{11\}$$

$$\mathrm{PS^{\bullet +} + {}^3O_2} \xrightarrow{\mathrm{k_{12}}} \mathrm{PS{-}OO^\bullet + H^+} \quad \{12\}$$

$$\mathrm{2\,{O_2}^{\bullet -} + 2\,H^+} \xrightarrow{\mathrm{k_{13}}} \mathrm{H_2O_2 + O_2} \quad \{13\}$$

$$\mathrm{H_2O_2 + h\nu} \xrightarrow{\mathrm{k_{14}}} \mathrm{2\,HO^\bullet} \quad \{14\}$$

$$\mathrm{2\,H_2O_2} \xrightarrow{\mathrm{k_{15}}} \mathrm{2\,H_2O + 2\,O_2} \quad \{15\}$$

$$\mathrm{pNDA + HO^\bullet} \xrightarrow{\mathrm{k_{16}}} \mathrm{-pNDA} \quad \{16\}$$

$$\mathrm{pNDA} \xrightarrow{\mathrm{k_9}} \mathrm{-pNDA} \quad \{9\}$$

Assuming than $\mathrm{PS^\bullet}$, $\mathrm{{O_2}^{\bullet -}}$ and $\mathrm{H_2O_2}$ are not stable because easily consumed (steady state hypothesis), we are writing $\frac{\mathrm{d[PS^\bullet]}}{\mathrm{d}t} = \frac{\mathrm{d[{O_2}^{\bullet -}]}}{\mathrm{d}t} = \frac{\mathrm{d[H_2O_2]}}{\mathrm{d}t} = 0$ and $v_{10} = v_{11} = 2v_{13} = 2v_{14} + 4v_{15}$. v_{15} is supposed to be very slow in front of v_{14} i.e. $v_{10} \approx 2v_{14}$. As $\mathrm{H_2O_2}$ is not stable and consumed by 14, we can write $2[\mathrm{H_2O_2}] = [\mathrm{HO^\bullet}]$.

Finally,

$$[\mathrm{HO^\bullet}] = \frac{k_{10}[\mathrm{PS}][\mathrm{PS^*}]}{k_{14}} \quad (4)$$

The interesting speed here is the rate of disappearance of pNDA, neglecting its auto-oxidation [9]. Therefore:

$$v = v_{16} = k_{16}[\mathrm{HO^\bullet}][\mathrm{pNDA}] \quad (5)$$

Therefore, with (4),

$$v = -\frac{\mathrm{d[pNDA]}}{\mathrm{d}t} = k_{16}[\mathrm{HO^\bullet}][\mathrm{pNDA}] = \frac{k_{16}k_{10}}{k_{14}}[\mathrm{PS}][\mathrm{PS^*}][\mathrm{pNDA}] = K[\mathrm{pNDA}] \quad (6)$$

with $\boxed{K = k_{16}[\mathrm{HO^\bullet}] = \frac{k_{16}k_{10}}{k_{14}}[\mathrm{PS}][\mathrm{PS^*}]}$.

The kinetic law is then linearizable via $\boxed{\ln \frac{[\mathrm{pNDA}]_0}{[\mathrm{pNDA}]_t} = Kt}$.

Remark : A dismutation of $-$pNDA has been proposed by [31], questioning the stoichiometry of 16 but the linearity of our experimental data seems to invalidate this hypothesis and we will then keep [19, 20] mechanistic hyposthesis.

2.6.3. Consideration of pNDA autooxidation

To consider pNDA autooxidation (16), we are supposing a first order kinetic law :

$$\text{pNDA} \xrightarrow{k_9} -\text{pNDA} \qquad \{9\}$$

Remark : to be more precise, autooxidation could also imply the others steps modifying PS by pNDA and PS* by pNDA*. In our experiment this point would only change the k_9 definition but do not modify the reasoning.

The general law (including singlet oxygen or radical and autobleaching) would be :

$$v = -\frac{\mathrm{d}[\text{pNDA}]}{\mathrm{d}t} = K[\text{pNDA}] + k_9[\text{pNDA}] = (K + k_9)\,[\text{pNDA}] = \kappa[\text{pNDA}] \quad (7)$$

with $\boxed{\kappa = K + k_9}$.

The kinetic law is then linearizable via $\boxed{\ln \frac{[\text{pNDA}]_0}{[\text{pNDA}]_t} = \kappa t}$.

The accessible kinetics are then k_9 (pNDA used alone) and κ (pNDA and sensitizor). To be precise, the contribution of the sensitizor is $K = \kappa - k_9$. In this document we are supposing $\kappa \approx K$ to simplify graphs, as k_9 was found negligible.

3. Results and discussion

3.1. Dosage Validation

The dosage validation was performed using MB as a photo sensitizer. MB is characterized by a strong absorption band in the 550–700 nm region with maximum molar absorptivity of 85,000 $\text{M}^{-1}.\text{cm}^{-1}$ at $\lambda = 664$ nm which justifies the irradiation by red LEDs in our experimental device. MB absorption spectrum is concentration-dependent due to dimerization (dimers have maximum absorption at 590 nm). To overcome these dimerization effects, we have used a MB concentration of 20 µM, for which only the monomer is present [25]. It is important to fix the pH in our studies because protonation of MB modify its photochemical properties and affect the efficiency of type I and type II photosensitization mechanisms. Consequently, in order to mimic a physiological pH, all our dosage were performed at pH = 7.4 (PBS buffer).

3.1.1. pNDA concentration range

The UV-vis spectrum of pNDA is given in Figure 11. The maximum of absorption is reached for $\lambda = 440$ nm and this absorption is linear, following the Beer-Lambert law, on a large concentration range. The intrinsic sensitivity of the spectrophotometer allowing a linear behavior for optical densities under 4, we are using pNDA in a concentration range of 0–100 µM.

3.1.2. pNDA autooxidation and reagents degradation

We evaluate the kinetics of pNDA auto-oxidation (k_9) by monitoring the effect of red light on a solution containing only pNDA (in PBS) with or without L-histidine. The auto-oxidation effect of pNDA is negligible on 15 minutes as no bleaching was detected. Before evaluating the assay as such, it is necessary to evaluate the potential degradation of the different reagents under irradiation. For this, each reagent is placed in the set up independently and in the concentration in which it will be used later. The dilution is carried out with PBS to ensure pH = 7.4. The absorption spectrum of the reagent in question is then regularly plotted and shown in Figure 12. For pNDA and L-histidine, the 15-minute irradiation does not significantly modify the optical density. For MB and BBG, a photochemical degradation is visible but around 440 nm, wavelength of study, this degradation correspond to a diminution of less than 0.01 in terms of optical density. pNDA presents, in our concentration range, an absorbance of 1.9 in this region. Thus, the degradation of MB, BBG and L-histidine is obviously negligible compared to the pNDA optical density. Therefore, all compounds degradation will be neglected, in comparison with the 440-nm pNDA bleaching.

3.1.3. Sensitivity and reproducibility

A typical assay describing the bleaching of pNDA induced by the irradiation of MB is shown in Figure 5. We are fitting the curves by a double exponential model as described previously. The first one describe the 60 first seconds of the dosage and gives an initial rate (continuous line) while the second one describe the 600 last seconds, giving an established rate (dashed line). This biphasic kinetic could not be explained by the photo-formation of absorbing products derived from L-histidine or MB. Indeed, a solution of L-histidine (5 mM) and MB (20 µM) under stirring and O_2 bubbling, irradiated for 20 minutes does not show the apparition of a new absorbing specie (Figure 12). Another possible explanation for this biphasic kinetic would be the formation of different pNDA adducts presenting various extinction coefficients. However, we were not able to characterize any of these pNDA adducts by electrospray mass spectrometry (data not shown).

Using the same conditions six times, we demonstrate the reproducibility of the dosage (more or less 2 basis-points) allowing the interpretation directly on the models (Figure 6). In the rest of this document, we will describe each photochemical reaction with two rates, namely initial and established rate. Note that the difference between oxidation in presence and in absence of L-histidine in the case of MB is clearly significant (6.4 times higher on average with $p = 5.769 \times 10^{-12}$), showing that MB is mainly but not only a type I photosensitizer ([29]).

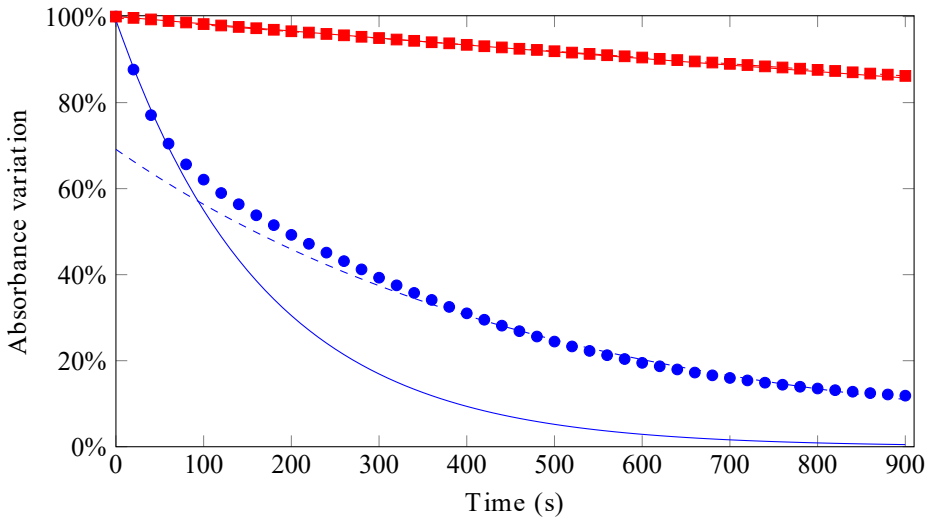

Figure 5: Normalized bleaching of the solution containing pNDA (90 µM), MB (20 µM) in PBS (pH = 7.4) with ● or without ■ L-histidine (5 mM) irradiated with red LEDs for 15 min. The different experiments data are shown by the geometrical shapes and their modeling is represented by the continuous line for initial rate and by the dashed line for established rate. All models are statistically significant ($p < 4 \times 10^{-3}$).

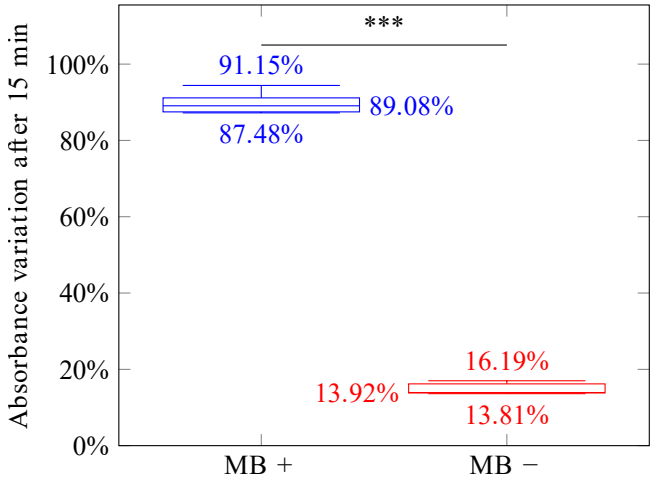

Figure 6: Normalized bleaching of the solution containing pNDA (90 µM), PBS (pH = 7.4) and MB (20 µM) with (+) ● or without (−) ● L-histidine (5 mM) after a red LEDs 15-minute irradiation. Each box is the average six experimental data. The numerical values shown are, from top to bottom, the upper quartile, the median and the lower quartile. All models are statistically significant ($p < 0.01$) and *** is for $p \leq 0.001$.

To detail this robustness a bit more, we compared the modeling slopes of the different experiments. The results are given in Figure 7. We can observe that, especially in the case of L-histidine presence, the variation on the result

mainly happens at the beginning of the reaction. Moreover, in the presence of L-histidine, the difference between initial rate and established one is important (2.5 fold in average) and significant (respectively $p = 1.101 \times 10^{-6}$). Without L-histidine, this difference is smaller even negligible (1.07 fold in average) and not significant ($p = 1.487 \times 10^{-1}$).

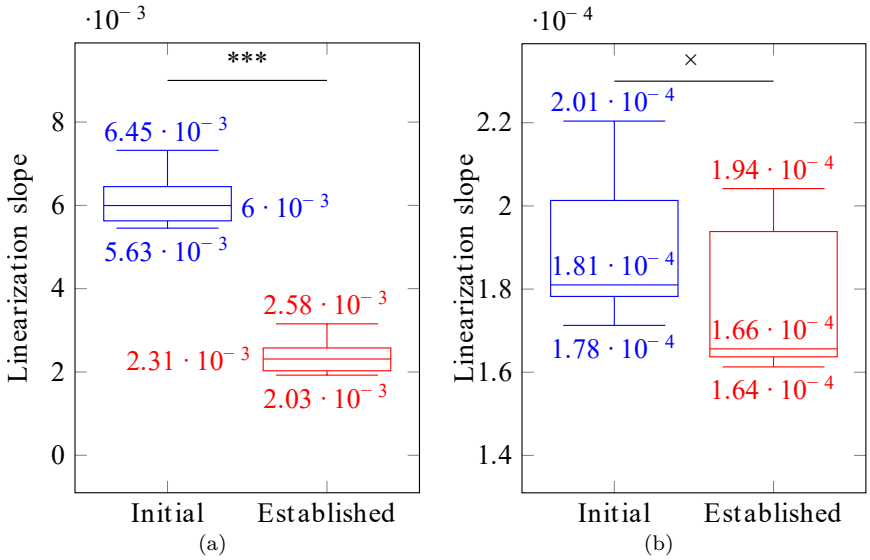

Figure 7: Linearization slopes of the bleaching of solutions containing pNDA (90 µM) and MB (40 µM) in PBS (pH = 7.4) with (a) or without (b) L-histidine (5 mM) irradiated with red LEDs for 15 min. Each data set is modeled with two limit cases of initial ● and established rate ●. Each box is the average six experimental data. The numerical values shown are, from top to bottom, the upper quartile, the median and the lower quartile. All models are statistically significant ($p < 0.001$) and × is for $p > 0.1$ and *** for $p \leq 0.001$.

3.2. Photochemical study

MB will remain our reference for this part. It has indeed several advantages. Firstly, its absorption is relatively weak and stable at 440 nm (cf. Figure 12) which simplifies the measurements and justifies the use of a fixed cell blank containing MB in its initial concentration during the flow measurement. Secondly, it presents a good quantum yield (around 0.52 in singlet oxygen production [32]) while keeping a simple chemical structure which facilitates its access. Finally, as mentioned previously, it is approved as a drug.

3.2.1. Independent determination of radicals and singlet oxygen

To ensure that the assay is selective for both hydroxyl radicals and singlet oxygen (in the presence of L-histidine), we performed a series of measurements

by adding a quencher of singlet oxygen. Based on results from the literature ([33, 34, 35]) we selected sodium azide. The protocol is the same as usual and the results are given in the Figure 8. The previous results on the variation of the assay on MB have been plotted on the two boxes on the left. The variation was significant (with a $p = 5.769 \times 10^{-12}$). The two right-hand columns are made with the presence of the quencher. No significant variation is observed since $p = 2.846 \times 10^{-1}$. This is consistent with the quenching of singlet oxygen by sodium azide. Unfortunately, we do not find exactly the same bleach without L-histidine with and without quencher, which should be the case if the quencher was ideal in terms of selectivity. Two points should be mentioned. First, the selectivity of the quencher is questioned in literature since it seems to react slightly with hydroxyl radicals [36]. Secondly, the variation between the two measurements is not strictly speaking perfectly significant. Indeed, the $p = 1.1 \times 10^{-2}$ shows that the two series are close. As a comparison, in the presence of L-histidine the variation between with and without quencher gives a $p = 4.754 \times 10^{-11}$.

As a conclusion of this study, the pNDA dosage is specific to hydroxyl radicals production without L-histidine and to singlet oxygen production with L-histidine.

3.2.2. Comparison with another sensitizer

Finally, we tried to compare MB to another sensitizer. The difficulty is to ensure the comparability of the data, through the reproduction of the experimental conditions. Thus, in order to keep our red LEDs crown, we chose a sensitizer with a color close to MB and we selected the BBG. To obtain comparable results, we prepared isoabsorbing solutions (20 µM MB and 17.5 µM BBG) at the excitation wavelength (630 nm), leading to absorbance of 0.585,6 and 0.584,8 respectively.

Different reasons have pushed us to choose the BBG, besides its simple color. This molecule is indeed part of the drug bank (DB15594) as *"a disclosing agent used in ophthalmological surgery to stain the internal limiting membrane"*. On the other hand, one publication described this molecule as photostable and without photosensitizing activity under white light irradiation [37]. It is therefore interesting to test our protocol on this product to confirm this conclusion under red light irradiation.

Therefore, we are using our standard conditions with MB and BBG and the results are precised in Figure 9. The variation in bleaching caused by the addition of L-histidine in the case of MB is still significant ($p = 5.769 \times 10^{-12}$), which is not really the case for BBG ($p = 2.297 \times 10^{-2}$). The analogous results between MB and BBG (either with or without L-histidine) are significant ($p = 1.829 \times 10^{-7}$ and $p = 4.845 \times 10^{-4}$ respectively). The very low bleaching due to BBG is comparable with the autobleaching of pNDA and can therefore be neglected, especially in the case of hydroxyl radical production, as mentioned by [37].

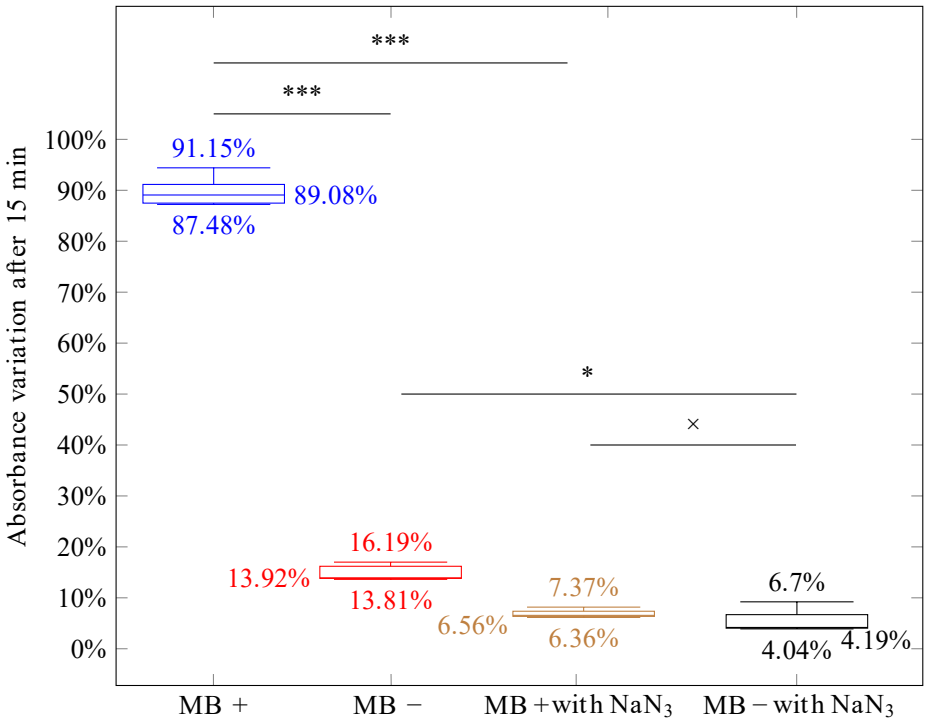

Figure 8: Normalized bleaching of the solution containing pNDA (90 µM) and MB (20 µM) in PBS (pH = 7.4) with (+) ● ● or without (−) ● ● L-histidine (5 mM) and with ● ● or without ● ● sodium azide (5 mM) after a red LEDs 15-minute irradiation. Each box is the average six experimental data without scavenger and three experimental data with scavenger. The numerical values shown are, from top to bottom, the upper quartile, the median and the lower quartile. All models are statistically significant ($p < 0.001$) and *** is for $p \leq 0.001$, * for $p \leq 0.05$ and × for $p > 0.1$.

These comparative results between MB and BBG show that MB is a much more sensitive photosensitizer than BBG regardless of the mechanism studied (type I electronic transfer or type II energy transfer). Nevertheless, to generalize this methodology to compare the ROS production efficiency of different PS, there is a need of various irradiation sources with the same photon production at the maximum wavelength of absorption of each photosensitizer.

4. Conclusion

This study made it possible to explore and validate the experimental conditions and reproducibility for the evaluation of hydroxyl radicals and singlet oxygen relative production efficiency by studying the bleaching of pNDA using a continuous flow UV-visible spectroscopy method in presence of a photosensitizer in PBS media. Rapid data sampling made possible to analyses the kinetic of the bleaching using a mathematical modeling. The pNDA dosage is specific of

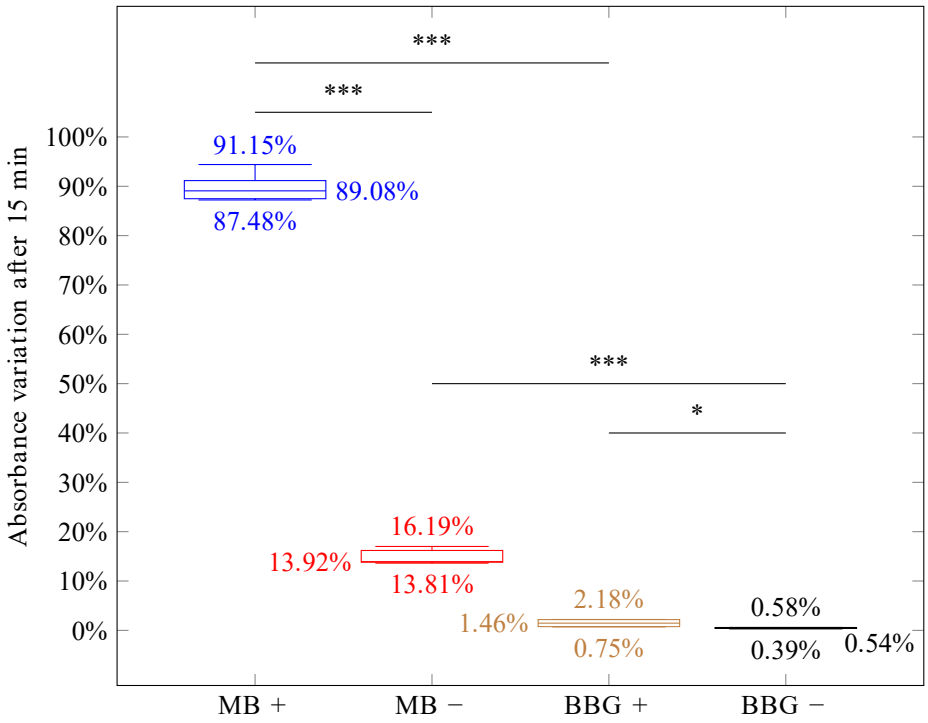

Figure 9: Normalized bleaching of the solution containing pNDA (90 µM) and MB (20 µM) ● ● or BBG (20 µM) ● ● in PBS (pH = 7.4) with (+) ● ● or without (−) ● ● L-histidine (5 mM) after a red LEDs 15-minute irradiation. Each box is the average six experimental data. The numerical values shown are, from top to bottom, the upper quartile, the median and the lower quartile. All model are statistically significant ($p < 0.001$) and *** is for $p \leq 0.001$ and * for $p \leq 0.05$.

hydroxyl radicals' production without L-histidine and of singlet oxygen production is with L-histidine. A statistical approach is used to precisely evaluate the reliability of the results and to be able to compare the efficiency of different photosensitizers such as MB and BBG and characterize their mechanism of generation of ROS via electron transfer (type I) or energy transfer (type II).

Acknowledgments

The authors thank Zacharias Amara and Fabienne Dioury for their experimental help in the degradation studies and for fruitful scientific discussions.

References

[1] J. Karges, Clinical development of metal complexes as photosensitizers for photodynamic therapy of cancer, Angew. Chem. Int. Ed. 61 (5). doi:10.1002/anie.202112236.

[2] S. Noimark, E. Salvadori, R. Gómez-Bombarelli, A. J. MacRobert, I. P. Parkin, C. W. M. Kay, Comparative study of singlet oxygen production by photosensitiser dyes encapsulated in silicone: towards rational design of antimicrobial surfaces, Phys. Chem. Chem. Phys. 18 (40) (2016) 28101–28109. doi:10.1039/C6CP02529C.

[3] C. Linger, G. Dumy, M. Port, Thérapie sonodynamique, Technologies biomédicales MED2000 v1. doi:10.51257/a-v1-med2000.

[4] T. C. Pham, V.-N. Nguyen, Y. Choi, S. Lee, J. Yoon, Recent strategies to develop innovative photosensitizers for enhanced photodynamic therapy, Chem. Rev. 121 (21) (2021) 13454–13619. doi:10.1021/acs.chemrev.1c00381.

[5] S. Kim, M. Fujitsuka, T. Majima, Photochemistry of singlet oxygen sensor green, J. Phys. Chem. B 117 (45) (2013) 13985–13992. doi:10.1021/jp406638g.

[6] S. K. Pedersen, J. Holmehave, F. H. Blaikie, A. Gollmer, T. Breitenbach, H. H. Jensen, P. R. Ogilby, Aarhus sensor green: A fluorescent probe for singlet oxygen, J. Org. Chem. 79 (7) (2014) 3079–3087. doi:10.1021/jo500219y.

[7] M. Galland, T. Le Bahers, A. Banyasz, N. Lascoux, A. Duperray, A. Grichine, R. Tripier, Y. Guyot, M. Maynadier, C. Nguyen, M. Gary-Bobo, C. Andraud, C. Monnereau, O. Maury, A "multi-heavy-atom" approach toward biphotonic photosensitizers with improved singlet-oxygen generation properties, Chem. Eur. J. 25 (38) (2019) 9026–9034. doi:https://doi.org/10.1002/chem.201901047.

[8] S. I. Dikalov, D. G. Harrison, Methods for detection of mitochondrial and cellular reactive oxygen species, Antioxid. Redox Signal. 20 (2) (2012) 372–382. doi:10.1089/ars.2012.4886.

[9] T. Entradas, S. Waldron, M. Volk, The detection sensitivity of commonly used singlet oxygen probes in aqueous environments, J. Photochem. Photobiol., B 204 (2020) 111787. doi:10.1016/j.jphotobiol.2020.111787.

[10] W. W. Grabow, Method for determination of singlet oxygen quantum yields for new fluorene-based photosensitizers in aqueous media for the advancement of photodynamic therapy (2004).
URL http://purl.fcla.edu/fcla/etd/CFE0000029

[11] V. Nardello, D. Brault, P. Chavalle, J.-M. Aubry, Measurement of photogenerated singlet oxygen ($^1O_2(^1Dg)$) in aqueous solution by specific chemical trapping with sodium 1,3-cyclohexadiene-1,4-diethanoate, J. Photochem. Photobiol., B 39 (2) (1997) 146–155. doi:10.1016/S1011-1344(97)00005-5.

[12] P. E. Hartman, Z. Hartman, K. T. Ault, Scavenging of singlet molecular oxygen by imidazole compounds: high and sustained activities of carboxy terminal histidine dipeptides and exceptional activity of imidazole-4-acetic acid, Photochem. Photobiol. 51 (1) (1990) 59–66. doi:10.1111/j.1751-1097.1990.tb01684.x.

[13] S. Goldstein, G. Czapski, Mannitol as an OH · scavenger in aqueous solutions and in biological systems, Int. J. Radiat. Biol. 46 (6) (1984) 725–729. doi:10.1080/09553008414551961.

[14] Y. Wang, R. Branicky, A. Noë, S. Hekimi, Superoxide dismutases: Dual roles in controlling ROS damage and regulating ROS signaling, J. Cell Biol. 217 (6) (2018) 1915–1928. doi:10.1083/jcb.201708007.

[15] Z. Zhang, Y. Si, G. Sun, Photoactivities of vitamin k derivatives and potential applications as daylight-activated antimicrobial agents, ACS Sustain. Chem. Eng. 7 (22) (2019) 18493–18504. doi:10.1021/acssuschemeng.9b04449.

[16] W. Bors, C. Michel, M. Saran, On the nature of biochemically generated hydroxyl radicals. studies using the bleaching of p-nitrosodimethylaniline as a direct assay method, Eur. J. Biochem. 95 (3) (1979) 621–627. doi:10.1111/j.1432-1033.1979.tb13003.x.

[17] Y.-W. Chen, T.-Y. Liu, P.-H. Chang, P.-H. Hsu, H.-L. Liu, H.-C. Lin, S.-Y. Chen, A theranostic nrGO@MSN-ION nanocarrier developed to enhance the combination effect of sonodynamic therapy and ultrasound hyperthermia for treating tumor, Nanoscale 8 (25) (2016) 12648–12657. doi:10.1039/C5NR07782F.

[18] N. Liu, G. Sun, Production of reactive oxygen species by photoactive anthraquinone compounds and their applications in wastewater treatment, Ind. Eng. Chem. Res. 50 (9) (2011) 5326–5333. doi:10.1021/ie101423v.

[19] C. Comninellis, Electrocatalysis in the electrochemical conversion/combustion of organic pollutants for waste water treatment, Electrochim. Acta 39 (11) (1994) 1857–1862. doi:10.1016/0013-4686(94)85175-1.

[20] M. E. Simonsen, J. Muff, L. R. Bennedsen, K. P. Kowalski, E. G. Søgaard, Photocatalytic bleaching of p-nitrosodimethylaniline and a comparison to the performance of other AOP technologies, J. Photochem. Photobiol. A 216 (2) (2010) 244–249. doi:10.1016/j.jphotochem.2010.07.008.

[21] I. Kraljić, S. E. Mohsni, A new method for the detection of singlet oxygen in aqueous solutions, Photochem. Photobiol. 28 (4) (1978) 577–581. doi:10.1111/j.1751-1097.1978.tb06972.x.

[22] V. V. Agon, W. A. Bubb, A. Wright, C. L. Hawkins, M. J. Davies, Sensitizer-mediated photooxidation of histidine residues: Evidence for the formation of reactive side-chain peroxides, Free Radic. Biol. Med. 40 (4) (2006) 698–710. doi:10.1016/j.freeradbiomed.2005.09.039.

[23] M. Boggio-Pasqua, J.-L. Heully, Thermolysis biradical mechanisms in endoperoxides: A challenge for density functional theory?, Theor. Chem. Acc. 135 (1) (2016) 9. doi:10.1007/s00214-015-1766-8.

[24] J.-M. Aubry, C. Pierlot, J. Rigaudy, R. Schmidt, Reversible binding of oxygen to aromatic compounds, Acc. Chem. Res. 36 (9) (2003) 668–675. doi:10.1021/ar010086g.

[25] J. P. Tardivo, A. Del Giglio, C. S. de Oliveira, D. S. Gabrielli, H. C. Junqueira, D. B. Tada, D. Severino, R. de Fátima Turchiello, M. S. Baptista, Methylene blue in photodynamic therapy: From basic mechanisms to clinical applications, Photodiagnosis Photodyn. Ther. 2 (3) (2005) 175–191. doi:10.1016/S1572-1000(05)00097-9.

[26] A. F. dos Santos, L. F. Terra, R. A. M. Wailemann, T. C. Oliveira, V. d. M. Gomes, M. F. Mineiro, F. C. Meotti, A. Bruni-Cardoso, M. S. Baptista, L. Labriola, Methylene blue photodynamic therapy induces selective and massive cell death in human breast cancer cells, BMC Cancer 17 (1) (2017) 194. doi:10.1186/s12885-017-3179-7.

[27] D.-J. Lim, Methylene blue-based nano and microparticles: Fabrication and applications in photodynamic therapy, Polymers 13 (22) (2021) 3955. doi:10.3390/polym13223955.

[28] M. Lam, C. Lam, J. Lam, Methylene blue as a photosensitizer in light therapy (2020).
URL https://www.drlamcoaching.com/blog/methylene-blue-as-a-photosensitizer/

[29] H. C. Junqueira, D. Severino, L. G. Dias, M. S. Gugliotti, M. S. Baptista, Modulation of methylene blue photochemical properties based on adsorption at aqueous micelle interfaces, Phys. Chem. Chem. Phys. 4 (11) (2002) 2320–2328. doi:10.1039/b109753a.

[30] M. F. Ruiz-López, M. T. C. Martins-Costa, J. S. Francisco, J. M. Anglada, Tight electrostatic regulation of the OH production rate from the photolysis of hydrogen peroxide adsorbed on surfaces, Proc. Natl. Acad. Sci. U.S.A. 118 (30) (2021) e2106117118. doi:10.1073/pnas.2106117118.

[31] J. Muff, L. R. Bennedsen, E. G. Søgaard, Study of electrochemical bleaching of p-nitrosodimethylaniline and its role as hydroxyl radical probe compound, J. Appl. Electrochem. 41 (5) (2011) 599–607. doi:10.1007/s10800-011-0268-1.

[32] G. A. Shahinyan, A. Y. Amirbekyan, S. A. Markarian, Photophysical properties of methylene blue in water and in aqueous solutions of dimethylsulfoxide, Spectrochim. Acta A Mol. Biomol. Spectrosc. 217 (2019) 170–175. doi:10.1016/j.saa.2019.03.079.

[33] S. Guo, X. Sun, J. Cheng, H. Xu, J. Dan, J. Shen, Q. Zhou, Y. Zhang, L. Meng, W. Cao, Y. Tian, Apoptosis of THP-1 macrophages induced by protoporphyrin IX-mediated sonodynamic therapy, Int. J. Nanomedicine 8 (2013) 2239–2246. doi:10.2147/IJN.S43717.

[34] J.-h. Li, D.-y. Song, Y.-g. Xu, Z. Huang, W. Yue, In vitro study of haematoporphyrin monomethyl ether-mediated sonodynamic effects on c6 glioma cells, Neurol. Sci. 29 (4) (2008) 229–235. doi:10.1007/s10072-008-0972-8.

[35] C. Ding, D. Xing, Studies on the sonosensitization mechanism of ultrasound with ATX-70 in sonodynamic therapy, in: B. Chance, M. Chen, A. E. T. Chiou, Q. Luo (Eds.), Photonics Asia 2004, 2005, pp. 639–646. doi:10.1117/12.572824.

[36] M. Bancirova, Sodium azide as a specific quencher of singlet oxygen during chemiluminescent detection by luminol and cypridina luciferin analogues: NaN3 as a quencher of 1o2 during CL detection by luminol and CLAs, Luminescence 26 (6) (2011) 685–688. doi:10.1002/bio.1296.

[37] K. Takayama, T. Sato, Y. Karasawa, S. Sato, M. Ito, M. Takeuchi, Phototoxicity of indocyanine green and brilliant blue g under continuous fluorescent illumination on cultured human retinal pigment epithelial cells, Invest. Ophthalmol. Vis. Sci. 53 (11) (2012) 7389. doi:10.1167/iovs.12-10754.

Appendix

Reagents generalities

Degradation spectra

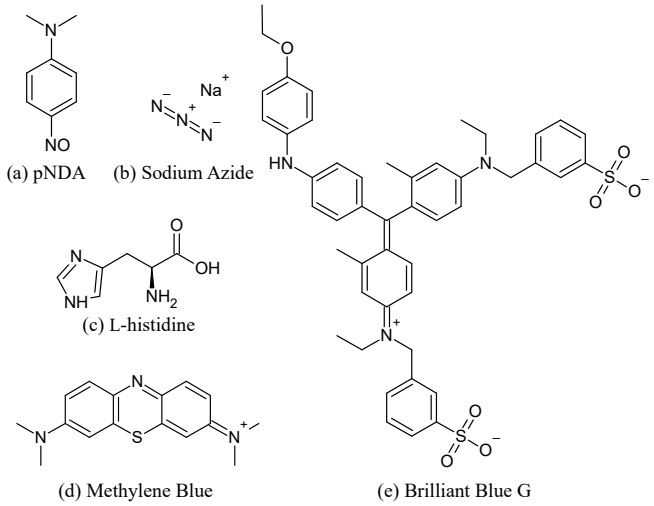

Figure 10: Principal Reagents Structure (and CAS). (a) *N*,*N*-dimethyl-4-nitrosoaniline (138-89-6). (b) sodium;azide (26628-22-8). (c) (2*S*)-2-amino-3-(1*H*-imidazol-5-yl)propanoic acid (71-00-1). (d) [7-(dimethylamino)phenothiazin-3-ylidene]-dimethylazanium;chloride (61-73-4). (e) sodium;3-[[4-[(*E*)-[4-(4-ethoxyanilino)phenyl]-[4-[ethyl-[(3-sulfonatophenyl)methyl]azaniumylidene]-2-methylcyclohexa-2,5-dien-1-ylidene]methyl]-N-ethyl-3-methylanilino]methyl]benzenesulfonate (6104-58-1).

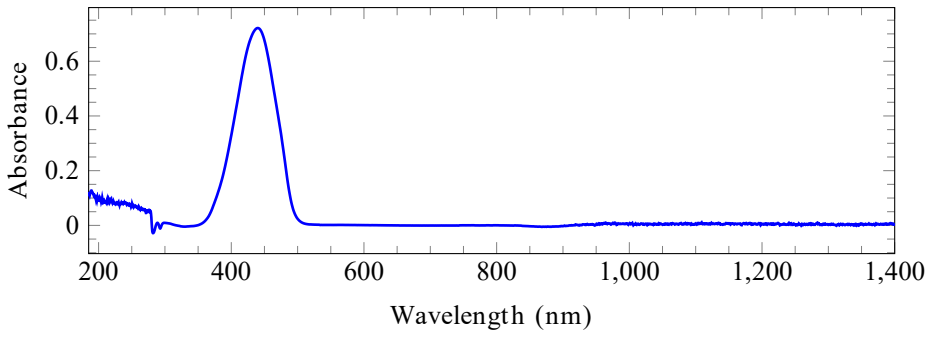

Figure 11: pNDA UV-vis spectrum (20 µM)

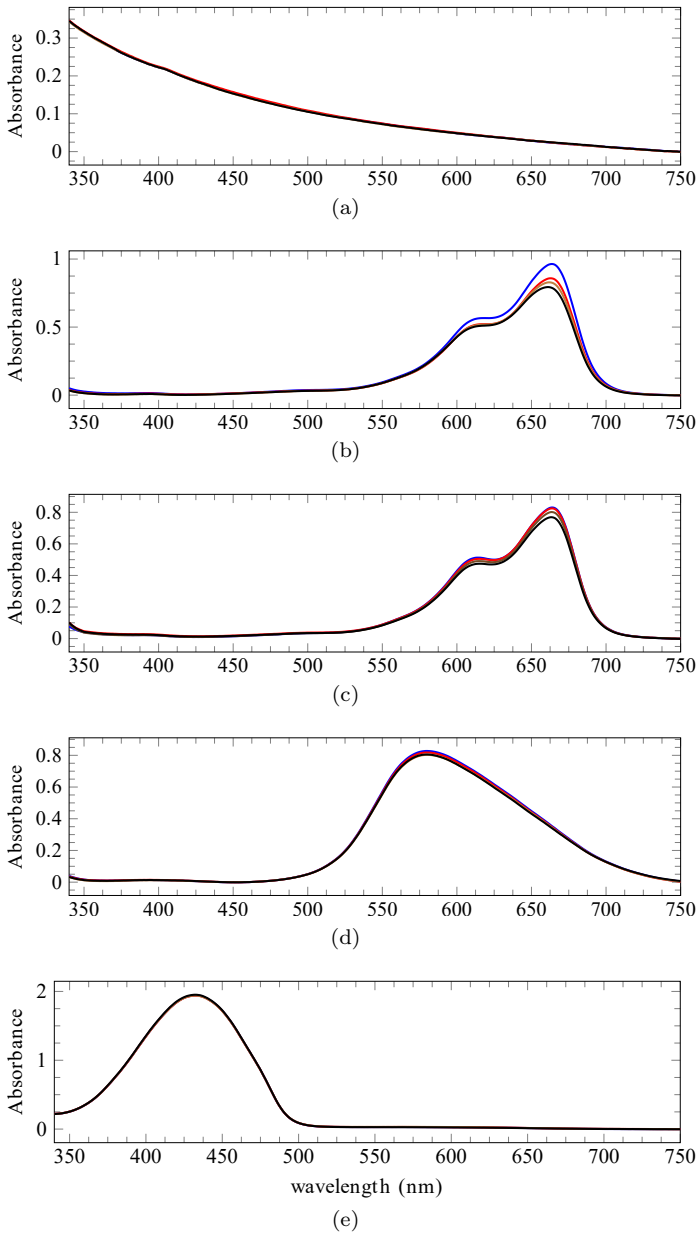

Figure 12: Degradation spectrum of (a) L-histidine (5 mM), (b) MB (20 µM), (c) MB (20 µM) and L-histidine (5 mM), (d) BBG (17.5 µM) and (e) pNDA (90 µM) under red LEDs irradiation, stirring and O_2 bubbling for 0 —, 5 —, 10 — and 20 min —.